PROCEEDINGS, Thirty-Eighth Workshop on Geothermal Reservoir Engineering
Stanford University, Stanford, California, February 11-13, 2013
SGP-TR-198

# COUPLED GEOMECHANICAL AND REACTIVE GEOCHEMICAL SIMULATIONS FOR FLUID AND HEAT FLOW IN ENHANCED GEOTHERMAL RESERVOIRS

Yi Xiong, Litang Hu and Yu-Shu Wu

Department of Petroleum Engineering
Colorado School of Mines
1500 Illinois Street,
Golden, CO, 80401, USA
e-mail: yxiong@mines.edu

## ABSTRACT

A major concern in development of fractured reservoirs in Enhanced Geothermal Systems (EGS) is to achieve and maintain adequate injectivity, while avoiding short-circuiting flow paths. The injection performance and flow paths are dominated by fracture rock permeability. The evolution of fracture permeability can be made by change in temperature or pressure induced rock deformation and geochemical reaction. Especially in fractured media, the change of fracture apertures due to geomechanical deformation and mineral precipitation/dissolution could have a major impact on reservoir long-term performance. A coupled thermal-hydrological-mechanical-chemical (THMC) model is in general necessary to examine the reservoir behavior in EGS.

This paper presents a numerical model, TOUGH2-EGS, for simulating coupled THMC processes in enhanced geothermal reservoirs. This simulator is built by coupling mean stress calculation and reactive geochemistry into the existing framework of TOUGH2 (Pruess et al., 1999), a well-established numerical simulator for geothermal reservoir simulation. The geomechanical model is fully-coupled as mean stress equations, which are solved simultaneously with fluid and heat flow equations. The flow velocity and phase saturations are used for reactive geochemical transport simulation after solution of the flow and heat equations in order to sequentially couple reactive geochemistry at each time step. The fractured medium is represented by multi interacting continua (MINC) model in the simulations.

We perform coupled THMC simulations to examine a prototypical EGS reservoir for fracture aperture change at the vicinity of the injection well. The results demonstrate the strong influence of temperature-induced rock deformation effects in the short-term and intermediate- and long-term influence of chemical effects. It is observed that the fracture enhancement by thermal-mechanical effect can be counteracted by the precipitation of minerals, initially dissolved into the low temperature injected water. We conclude that the temperature and chemical composition of injected water can be modified to improve reservoir performance by maintaining or even enhancing fracture network under both geomechanical and reactive geochemical effects.

## INTRODUCTION

The successful development of enhanced geothermal systems (EGS) highly depends on the reservoir fracture network of hot dry rock (HDR) and its hydraulic properties. The geomechanical processes under subsurface reservoir condition are prevalent in the EGS applications. For example, Tsang and Chin-Fu (1999) presented that hydraulic properties of fracture rocks are subjected to change under reservoir mechanical effects. Rutqvist et al. (2002) investigated the stress-induced changes in the fracture porosity, permeability and capillary pressure. It is also well known that the cold water injection and steam or hot water extraction have thermo-poro-elastic effects for EGS reservoirs.

On the other hand, the strong impacts of geochemical reaction on the EGS reservoirs have been observed in the commercial EGS fields in the past few years. Kiryukhin et al.(2004) modeled the reactive chemical process based on the field data from tens of geothermal fields in Kamchatka (Russia) and Japan. In addition, Xu et al. (2004a) presented the reactive transport model of injection well scaling and acidizing at Tiwi field in Philippines. Montalvo et al. (2005) studied the calcite and silica scaling problems with exploratory model for Ahuachapan and Berlin geothermal fields in El Salvador. The typical chemical reactions between fluids and rock minerals

in EGS reservoirs, the mineral dissolution and precipitation, should be fully evaluated and predicted in order to assist the development of geothermal energy.

The numerical simulation is a powerful tool to model the geomechanical and geochemical processes for EGS reservoirs. The research efforts have been put in this direction and a few EGS reservoir simulation tools are developed. For example, Rutqvist et al. (2002) linked TOUGH2 (Pruess et al., 1999) and FLAC3D for modeling of THM process. Wang and Ghassemi (2012) presented a 3D thermal-poroelastic model for geothermal reservoir simulation. Fakcharoenphol and Wu (2012) developed the fully implicit flow and geomechanics model for EGS reservoirs. The coupled THC simulator, TOUGHREACT (Xu et al., 2004b), has the capability to model the multi-components multi-phase fluid flow, solute transport and chemical reactions in the subsurface systems. However, the single programs coupling THMC processes are rarely available. Taron et al. (2009) introduced one "modular" approach to generate a coupled THMC simulator by coupling the capabilities of TOUGHREACT with the mechanical framework of FLAC3D. Compared with single coupled program, although the modular approach may be more rapid and less expensive, it may result in the issues of flexibility and accuracy.

In this paper, we present one single coupled THMC simulator for geothermal reservoir modeling, TOUGH2-EGS. This simulator is built by coupling mean stress calculation and geochemical reactions into the existing framework of TOUGH2 (Pruess et al., 1999), a well-established numerical simulator for subsurface thermal-hydrological analysis with multi-phase, multi-component fluid and heat flow. The mechanical model is fully-coupled as the mean stress equations, solved simultaneously with fluid and heat flow equations. In order to sequentially couple the chemical process, the solution of fluid and heat flow equations provides the flow velocity and phase saturation to compute the solute transport and chemical reactions at each time step.

This paper is organized as follows. First, we present the mathematical model for coupling geomechanical and geochemical processes. Then the simulation procedure for coupling THMC processes is introduced. Finally, one application example for simulating the THMC processes at the vicinity of the injection well is presented. In this application example, we analyze the fracture aperture evolution due to the mechanical and chemical effects through three cases. By comparing the base case and modified cases, it is found that the mechanical and chemical process may be in favor of or undermine the fracture network by modifying chemical components and temperature of the injection water.

## MATHEMATICAL MODEL

### Formulation of Fluid and Heat Flow

The fluid and heat flow equations are formulated based on mass and energy conservation. Following the integral formats of TOUGH2, the general mass and energy balance equation can be written as

$$\frac{d}{dt}\int_{V_n} M^k dV_n = \int_{\Gamma_n} \bar{F}^k \cdot \hat{n} d\Gamma_n + \int_{V_n} q^k dV_n \qquad (1)$$

The integration is over an arbitrary subdomain or representative element volume (REV) $V_n$ of EGS reservoir flow system, which is bounded by the closed surface $\Gamma_n$. The quantity $M$ in the accumulation term represents mass or energy per volume, with $k$=1, 2 labeling the component of water and air in the EGS reservoir and $k$=3 labeling heat "component" for energy balance. $F$ donates the mass or heat flux, and $q$ donates sinks and sources. $n$ is the normal vector on the surface element $d\Gamma_n$, pointing inward into $V_n$. The general form of mass accumulation for component $k$ is

$$M^k = \phi \sum_\beta S_\beta \rho_\beta X_\beta^k \qquad (2)$$

The total mass of component $k$ is obtained by summing over the fluid phase $\beta$ (= liquid or gas). $\phi$ is the porosity, $S_\beta$ is the saturation of phase $\beta$, $\rho_\beta$ is the density of phase $\beta$, and $X_\beta^k$ is the mass fraction of component $k$ present in phase $\beta$. Similarly the heat accumulation is

$$M^{k=3} = (1-\phi)\rho_R C_R T + \phi \sum_\beta S_\beta \rho_\beta u_\beta \qquad (3)$$

where $\rho_R$ and $C_R$ is the grain density and specific heat of the rock. $T$ is the temperature and $u_\beta$ is the specific internal energy in phase $\beta$.

The mass flux includes advective and diffusive flux (hydrodynamic dispersion and molecular diffusion) as

$$F^k = F_{adv}^k + F_{dis}^k \qquad (4)$$

Advective flux is the sum over phases,

$$F_{adv}^k = \sum_\beta X_\beta^k F_\beta \qquad (5)$$

The advective flux of phase $\beta$ is given by the multiphase Darcy's law as

$$F_\beta = \rho_\beta v_\beta = -k\frac{k_{r\beta}\rho_\beta}{\mu_\beta}\left(\nabla P_\beta - \rho_\beta g\right) \quad (6)$$

where $v_\beta$ is Darcy velocity of phase $\beta$, $k$ is the absolute permeability; $k_{r\beta}$ and $\mu_\beta$ are relative permeability and viscosity of phase $\beta$ respectively. $P_\beta$ is the fluid pressure of the phase, which is given by the pressure of reference phase and the capillary pressure between the phases.

In addition to the advective flow, the mass transport also occurs through hydrodynamic dispersion and molecular diffusion defined as follows.

$$F^k_{disp} = -\sum_\beta \rho_\beta \bar{D}^k_\beta \nabla X^k_\beta \quad (7)$$

$$F^k_{diff} = -\phi\tau_0\tau_\beta\rho_\beta d^k_\beta \nabla X^k_\beta \quad (8)$$

$$F^k_{dis} = F^k_{disp} + F^k_{diff} \quad (9)$$

where $D_\beta{}^k$ is the hydrodynamic dispersion tensor; $d_\beta{}^k$ is the molecular diffusion coefficient for component $k$ in phase $\beta$. $\tau_0$ and $\tau_\beta$ are the tortuosity factors, respectively depending on rock property and phase saturation.

The heat flow is governed by conduction and convection.

$$F^{k=3} = -\lambda\nabla T + \sum_\beta h_\beta F_\beta \quad (10)$$

where $\lambda$ is thermal conductivity, and $h_\beta$ is specific enthalpy in phase $\beta$. $F_\beta$ is given by equation (6).

**Formulation of Geomechanics**

The fully coupled mechanical model assumes that each grid block can move as an elastic material and obey the generalized Hooke's law.

Under the assumption of linear elastic with small strain for thermo-poro-elastic system, the stress equilibrium can be expressed as follows (Jaeger et al., 2007, Winterfeld and Wu, 2011)

$$\sigma_{kk} - \left(\alpha P + 3\beta K\left(T - T_{ref}\right)\right) = \lambda\left(\varepsilon_{xx} + \varepsilon_{yy} + \varepsilon_{zz}\right) + 2G\varepsilon_{kk}, k = x, y, z \quad (11)$$

where $\sigma$ is the normal stress, $\alpha$ is the Biot's coefficient, $\beta$ is the linear thermal expansion coefficient, $K$ is the bulk modulus, $\lambda$ is the Lame's constant, $G$ is the shear modulus and $\varepsilon$ is the strain. The subscript $k$ stands for the directions.

Summing over the $x$, $y$ and $z$ component of equation (11) gives the trace of Hooke's law for poroelastic medium.

$$\frac{\sigma_{xx} + \sigma_{yy} + \sigma_{zz}}{3} - \alpha P - 3\beta K\left(T - T_{ref}\right) = \left(\lambda + \frac{2}{3}G\right)\left(\varepsilon_{xx} + \varepsilon_{yy} + \varepsilon_{zz}\right) \quad (12)$$

Rewrite equation (12) in terms of mean normal stress and volumetric strain as

$$\sigma_m - \alpha P - 3\beta K\left(T - T_{ref}\right) = \left(\lambda + \frac{2}{3}G\right)\varepsilon_v \quad (13)$$

where $\sigma_m$ and $\varepsilon_v$ are the mean normal stress and volumetric strain.

The poroelastic version of the Navier equations may be written as

$$\alpha\nabla P + 3\beta K\nabla T + \left(\lambda + G\right)\nabla\left(\nabla\cdot\bar{u}\right) + G\nabla^2\bar{u} + \bar{F} = 0 \quad (14)$$

where $\bar{u}$ is the displacement vector and $\bar{F}$ is the body force. The divergence of the displacement vector is the volumetric strain as

$$\nabla\cdot\bar{u} = \frac{\partial u_x}{\partial x} + \frac{\partial u_y}{\partial y} + \frac{\partial u_z}{\partial z} = \varepsilon_{xx} + \varepsilon_{yy} + \varepsilon_{zz} = \varepsilon_v \quad (15)$$

Take partial derivatives with respect to $x$ for the x-component of equation (14), with respect to $y$ for the y-component and with respect to $z$ for the z-component, and add together to achieve the following equation.

$$\alpha\nabla^2 P + 3\beta K\nabla^2 T + \left(\lambda + 2G\right)\nabla^2\left(\nabla\cdot\bar{u}\right) + \nabla\cdot\bar{F} = 0 \quad (16)$$

Solving $\varepsilon_v$ in equation (13) and substitute $\nabla\cdot\bar{u}$ in equation (16) gives us the governing equation coupling pore pressure, temperature and mean normal stress.

$$\frac{3(1-\nu)}{(1+\nu)}\nabla^2\sigma_m + \nabla\cdot\bar{F} = \frac{2(1-2\nu)}{(1+\nu)}\left(\alpha\nabla^2 P + 3\beta K\nabla^2 T\right) \quad (17)$$

where $\upsilon$ is the Poisson's ratio, substituting the $\lambda$ and $G$ of the original equations with the appropriate relationships.

The multiple interacting continua (MINC) approach (Pruess and Narasimhan, 1985) is used to simulate facture and matrix flow and interactions in our model. From the dual porosity poroelastic Navier equations (Bai and Roegiers, 1994) with the similar steps as before, the governing geomechanical

equation for each set of MINC blocks can be derived as

$$\frac{3(1-\nu)}{(1+\nu)}\nabla^2\sigma_m+\nabla\cdot\bar{F}=\frac{2(1-2\nu)}{(1+\nu)}\sum_{i=1}^{N}\left(\alpha_i\nabla^2P_i+3\beta_iK\nabla^2T_i\right) \quad (18)$$

where $N$ is the total number of MINC blocks for each set.

**Formulation of Reactive Chemistry**

Due to the complexity of multiphase fluid and heat flow, fluid-rock interaction and the strong non-linearity in mass and energy conservation equation for geochemical process, it is costly to develop the fully coupled chemical reaction model (Zhang et al., 2012). We therefore take the approach same as the TOUGHREACT to sequentially couple the chemical reaction process, which iteratively solves solute transport and chemical reactions.

***Solute transport***

The solute transport occurring in the liquid phase also follows the general mass balance equation (1), where accumulation and flux terms may be expressed

$$M^k=\phi S_kC_{kl} \quad (19)$$

$$F^k=v_lC_{kl}-\left(\tau\phi S_lD_l\right)\nabla C_{kl} \qquad k=1...N_l \quad (20)$$

where $N_l$ is the total number of the chemical components (species) in the liquid phase; $C_{kl}$ is the concentration of the $k^{th}$ species in liquid phase; $v_l$ is the Darcy velocity, $D_l$ is the diffusion coefficient.

It is convenient to select a subset of aqueous species as basis species (primary species) for representing a geochemical system. All other species, including aqueous complexes, precipitated species, are called secondary species. The number of secondary species must be equal to the number of independent reactions. Any of the secondary species can be represented as a linear combination of basis species as

$$C_i=\sum_{j=1}^{N_c}v_{ij}C_j \qquad i=1...N_R \quad (21)$$

where $N_c$ is the number of the primary species and $N_R$ is the number of the secondary species, $j$ is the primary species index and $i$ is the secondary species index, $v_{ij}$ is the stoichiometric coefficient of $j^{th}$ primary species in the $i^{th}$ reaction. Likewise, the concentration of aqueous complex can be expressed as function of that of primary species

$$c_i=K_i^{-1}\gamma_i^{-1}\prod_{j=1}^{N_c}c_j^{v_{ij}}\gamma_j^{v_{ij}} \quad (22)$$

where $c_i$ is the concentration of the $i^{th}$ aqueous complex, and $c_j$ is the concentration of the $j^{th}$ primary species, $\gamma$ is the thermodynamic activity coefficients and $K_i$ is the equilibrium constant. Therefore it is sufficient to only solve primary species concentration in the transport solute; the secondary species and aqueous complex can be readily represented.

***Mineral dissolution/precipitation***

The mineral saturation ratio can be expressed as

$$\Omega_m=X_m^{-1}\lambda_m^{-1}K_m^{-1}\prod_{j=1}^{N_c}c_j^{v_{mj}}\gamma_j^{mj} \qquad m=1...N_p \quad (23)$$

where $N_p$ is the number of minerals at equilibrium conditions, $m$ is he equilibrium mineral index, $\Omega_m$ is mineral saturation ratio, $X_m$ is the mole fraction of the $m^{th}$ mineral phase, $\lambda_m$ is its thermodynamic activity coefficient ($X_m$ and $\lambda_m$ are taken to one for pure mineral phases), and $K_m$ is the corresponding equilibrium constant. At equilibrium condition

$$SI_m=Log\Omega_m=0 \quad (24)$$

where $SI_m$ is the mineral saturation index.

For the kinetic mineral dissolution/precipitation, the kinetic rate could be functions of non-primary species. We usually consider the species appearing in rate laws as the primary species. In our model, we use the rate expression given by Lasaga et al. (1994),

$$r_n=f\left(c_1,c_2,...,c_{Nc}\right)=\pm k_nA_n\left|1-\Omega_n^{\theta}\right|^{\eta} \qquad n=1...N_q \quad (25)$$

where $N_q$ is the number of minerals at kinetic conditions, the positive values of $r_n$ indicate dissolution and negative values for precipitation, $k_n$ is the rate constant (moles per unit mineral surface area and unit time) which depends on the temperature, $A_n$ is the specific reactive surface area per kg $H_2O$. $\Omega_n$ is the kinetic mineral saturation ratio defined as equation (23). The parameters $\theta$ and $\eta$, can be determined from experiment, usually assumed to be unity. The reaction rate constant $k_n$ is dependent on temperature and usually rate constants are reported at 25°C. For a reasonable approximation, the rate constant could be handled via the Arrhenius equation (Lasaga 1984; Steefel and Lasaga 1994),

$$k=k_{25}\exp\left[\frac{-E_a}{R}\left(\frac{1}{T}-\frac{1}{298.15}\right)\right] \quad (26)$$

where $E_a$ is the activation energy, $k_{25}$ is the rate constant at 25°C, $R$ is gas constant, $T$ is absolute temperature.

**Numerical Model**

The general mass and energy balance equation (1) is discretized in space using integral finite difference method (IFD; Narasimhan and Witherspoon, 1976). By introducing proper average volume and approximating surface integrals to a discrete sum of averages over surface segments, the equation (1) has the residual form as equation (27) with time and space discretization.

$$R_n^{k,t+1} = M_n^{k,t+1} - M_n^{k,t} - \frac{\Delta t}{V_n}\left[\sum_m A_{nm} F_{nm}^{k,t+1} + V_n q_n^{k,t+1}\right] = 0 \quad (27)$$

where $R$ is the residual of component $k$ ( $k$ = 1 and 2 stands for components of water and air, and 3 stands for the heat) for grid block $n$, $t+1$ donates the current time level, $m$ donates the neighboring grid blocks of $n$, $A_{nm}$ and $F_{nm}$ are the interface area and flux between them.

In order to fully couple the geomechanical effect, the mean stress governing equation (17) needs to be discretized to the same form as equation (27). Applying the divergence theorem and approximating surface integrals to a discrete sum over surface segments, the mean stress equation has the following discretized residual form,

$$R_n^{4,t+1} = \sum_m \left[\frac{3(1-\nu)}{(1+\nu)}\nabla\sigma + \bar{F} - \frac{2(1-2\nu)}{(1+\nu)}\left(\alpha\nabla P + 3\beta K\nabla T\right)\right] A_{nm} = 0 \quad (28)$$

where $m$ is the neighboring grid blocks of $n$ and $A_{nm}$ is the interface area between them. There are total four residual equations with four primary variable, pressure, temperature, air mass fraction and mean normal stress, which are solved simultaneously through Newton-Raphson methods. After solving the THM process, the Darcy velocity and phase saturation are used to compute solute transport and chemical reaction, which also follows a similar numerical method.

**RESERVOIR EVOLUTION UNDER THMC EFFECTS**

The EGS reservoir properties, such as permeability, porosity, block volume, and capillaries etc., are subject to changes under the geomechanical and geochemical effects, and those changes may feedback to the heat and fluid flows. The relationship between effective stress $\sigma'$ and permeability $k$, porosity $\phi$ has been investigated through many research efforts (Ostensen et al., 1986; McKee et al., 1988; Davies and Davies, 2001; Rutqvist et al., 2002).

$$k = k(\sigma') \qquad \phi = \phi(\sigma') \quad (29)$$

Our mechanical model implements those correlations and the user can choose the proper one according to the specific reservoir conditions.

The geochemical model considers the porosity change due to mineral dissolution/precipitation as follows.

$$\phi_c = 1 - \sum_{m=1}^{Nm} fr^m - fr^u \quad (30)$$

where $N_m$ is the number of reactive minerals and $fr^m$ is the mineral fraction in the containing rock ($V_{mineral}/V_{medium}$), $fr^u$ is the non-reactive fraction. Since $fr^m$ of each mineral change, the porosity is updated at each time step.

The above analysis applies to the independent THM or THC processes. As for the THMC process, we combine the fracture aperture change due to both mechanical and chemical processes. The aperture under the effective stress $\sigma'$ may be defined empirically as (Rutqvist et al., 2002)

$$b_m = b_i + \Delta b_m = b_i + b_{\max}\left[\exp(-d\sigma') - \exp(-d\sigma_i')\right] \quad (31)$$

where $b_m$ is the aperture under mechanical effect, $b_i$ is the initial aperture under no stress, $b_{max}$ is maximum "mechanical" aperture and $d$ is the constant defining the non-linear stiffness of the fracture, $\sigma'$ and $\sigma_i'$ are the current stress and initial stress. On the other hand, chemical dissolution and precipitation could lead to the change in fracture aperture $\Delta b_c$ under chemical effect (Xu et al., 2004b).

$$\Delta b_c = \frac{\phi_c - \phi_c^0}{\phi_c^0} b_g \quad (32)$$

$$b_g = \frac{\phi_f^0}{A_f} \quad (33)$$

where $b_g$ is the initial aperture available for precipitation (geometry aperture), which can be calculate from the ratio of the initial fracture porosity $\phi_f^0$ to the fracture surface area $A_f$. The total aperture under THMC effects therefore is

$$b^{t+1} = b^t + \Delta b_m^{t+1} + \Delta b_c^{t+1} \quad (34)$$

where the $t+1$ and $t$ means current and previous time step; subscripts $m$ and $c$ means the mechanical and chemical effects respectively. The changed fracture

aperture leads to the updated permeability, porosity and capillary pressure. The possible relationships between them are

$$k^{t+1} = \frac{\left(b^{t+1}\right)^3}{12W} \tag{35}$$

$$\phi^{t+1} = \phi_0 \frac{b_1^{t+1} + b_2^{t+1} + b_3^{t+1}}{b_1^0 + b_2^0 + b_3^0} \tag{36}$$

$$p_c = p_c^0 \sqrt{\frac{k^0 \phi}{k \phi^0}} \tag{37}$$

where equation (35) is the cubic law (Snow, 1969; Witherspoon et al., 1979) and *W* is the fracture space; Rutqvist et al. (2002) derived equation (36) with cubic-block conceptual model, and used J-function to correct capillary pressure as equation (37). The superscripts *t+1* is the current time step and *0* is the initial time.

## SIMULATION LOGIC AND PROCEDURE

Our EGS reservoir simulator is a single program built on the framework of TOUGH2, fully coupling geomechanics and sequentially coupling reactive geochemistry. The figure 1 describes the program process. It mainly includes two modules, the geomechanical and geochemical modules. Although the figure shows the THMC process, the two modules could be run independently only for THM or THC according to the selection in the input files.

The THMC coupling logic is as follows: The input files, including rock hydrologic and geomechanical properties, computing parameters, solute and chemical parameters, etc. are read into the program. Before stepping into the main cycle, the program initializes the stress state and chemical state variables at initial condition. For each time step, the THM variables are firstly solved and the results, such as fluid velocity, phase saturations and temperature distributions, will be used to solve solute transport and chemical reactions. The solute transport and chemical reactions are solved iteratively until chemical state converges. The time control cycle repeats until the target time is reached.

## APPLICATION AND DISCUSSION

In the application example, we present one prototypical EGS reservoir to simulate THMC process of the vicinity of the injection well. As shown in the figure 2, the fractured reservoir is overlain by the caprock and the injection well is in the middle of the simulated area. The mesh is generated with radial and vertical (R-Z) dimensions and logarithmic distribution in radial direction to capture the subtle effects around the wellbore. The tables 1 and 2 list the reservoir mechanical and chemical properties.

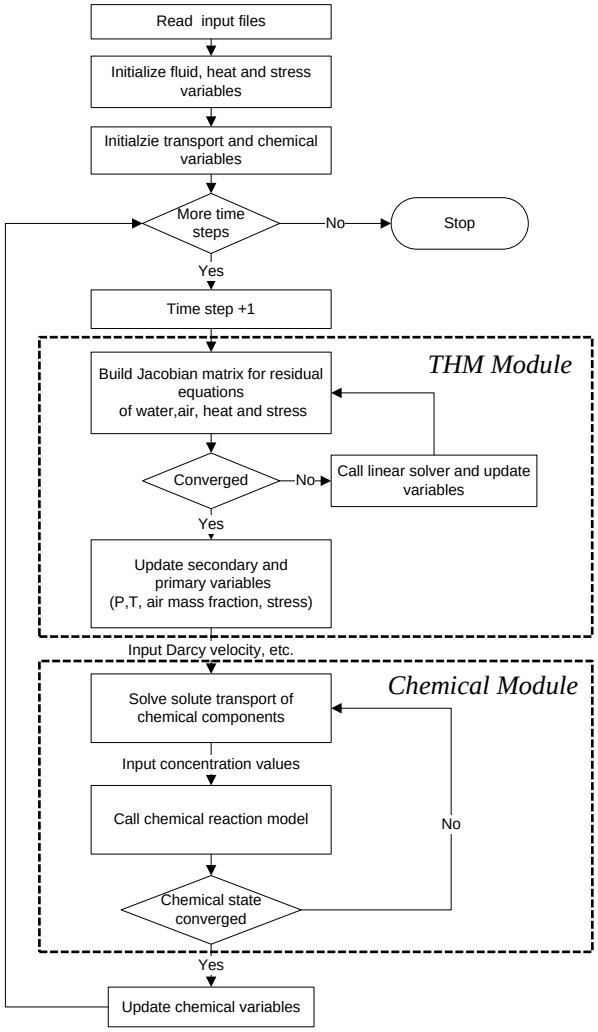


*Figure 1: Simulation process for THMC coupling*

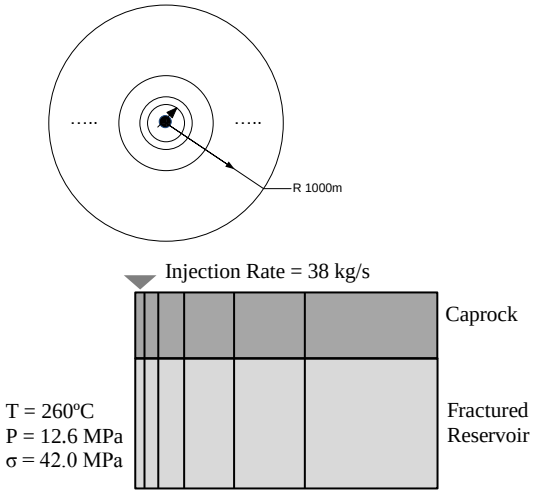


*Figure 2: Geometry of the simulated area and initial temperature, pressure and mean stress*

*Table 1: Reservoir and material properties*

| Properties | Values |
|---|---|
| Young's Modulus *(GPa)* | 14.4 |
| Poisson's ratio *(dimensionless)* | 0.20 |
| Permeability *($m^2$)* | $2.37\times10^{-13}$ |
| Porosity *(dimensionless)* | 0.1 |
| Pore compressibility*($Pa^{-1}$)* | $5\times10^{-10}$ |
| Thermal expansion coefficient *($^oC^{-1}$)* | $4.14\times10^{-6}$ |
| Rock grain specific heat *(J/kg $^oC$)* | 1000 |
| Rock grain density *(kg/$m^3$)* | 2750 |
| Formation thermal conductivity *(W/m $^oC$)* | 2.4 |
| Constant *d* in Eq. (31) *($Pa^{-1}$)* | $1.06\times10^{-7}$ |
| Maximum aperture in Eq. (31) (m) | $1.86\times10^{-4}$ |
| Geometry aperture in Eq. (32) (m) | $1.55\times10^{-3}$ |
| Biot's coefficient *(dimensionless)* | 1.0 |

*Table 2: The chemical components for reservoir initial water and injection water*

| Chemical Species | Initial Water Concentration (mol/l) | Injection Water Concentration (mol/l) |
|---|---|---|
| $Ca^{2+}$ | $3.32\times10^{-3}$ | $1.0327\times10^{-3}$ |
| $Mg^{2+}$ | $8.62\times10^{-6}$ | $1.6609\times10^{-6}$ |
| $Na^{+}$ | $1.285\times10^{-1}$ | $1.2734\times10^{-1}$ |
| $Cl^{-}$ | $1.418\times10^{-1}$ | $1.418\times10^{-1}$ |
| $SiO_2$(aq) | $1.218\times10^{-2}$ | $1.1734\times10^{-2}$ |
| $HCO_3^{-}$ | $1.0423\times10^{-3}$ | $1.0423\times10^{-3}$ |
| $SO_4^{2-}$ | $2.6272\times10^{-4}$ | $2.6272\times10^{-4}$ |
| $K^{+}$ | $1.5852\times10^{-2}$ | $1.5852\times10^{-2}$ |
| $AlO_2^{-}$ | $0.059\times10^{-4}$ | $0.0205\times10^{-4}$ |

The figure 3 shows the initial mineral composition of reservoir rock by volume fractions. The volume fraction of the mineral is the mineral volume divided by total volume of solids, excluding the liquid volume. The sum of the mineral volume fraction is not necessary to be 1 because the remaining solid fraction is considered to be un-reactive throughout the whole process.

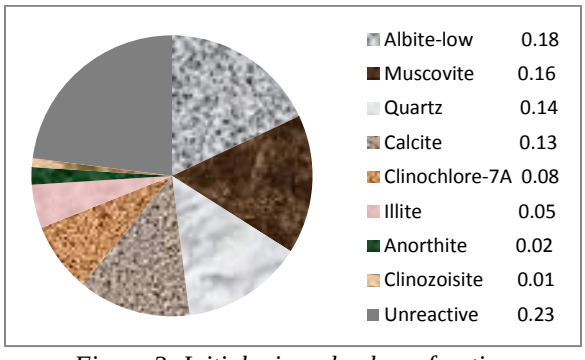


*Figure 3: Initial mineral volume fraction*

In order to represent a prototypical EGS reservoir, the geomechanical and geochemical data are taken from reasonable assumptions and from the Tiwi EGS field of Philippines (Xu et al., 2004a; Takeno et al., 2000). We run three simulation cases within one year to investigate the THMC effects with changed chemical composition and temperature of the injection water. The base case has the injection temperature of 150 $^o$C and chemical concentrations as table 2. The case 1 has the same injection temperature but lower concentration of aqueous $SiO_2$ in the injection water. The case 2 has the same chemical concentration as table 2 but with lower injection temperature of 120$^o$C.

**Base Case**

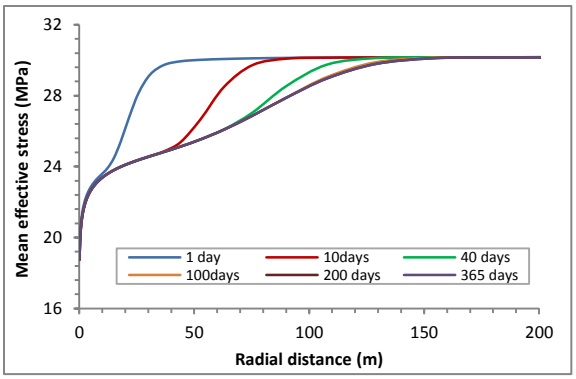


*Figure 4: Reservoir effective mean stress evolution*

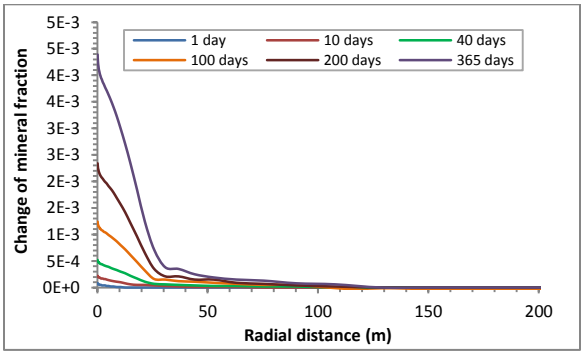


*Figure 5: Mineral volume fraction evolution*

Figures 4 and 5 show the evolution of geomechanical and geochemical states extending to 200m from the injection well simulated in one year. The mechanical and chemical effects on the reservoir are spatially and temporally different. Spatially, the mechanical effect has larger impacts on the area of radius about 150m and chemical impacts on that of radius about 30m from injection well in one year study. Temporally, the mean effective stress keeps decrease from day 1 to end of the simulation, but the remarkable change happens in the early time before 40 days. The stress state is almost unchanged after 100 days. With respect to the chemical state, the positive change of mineral fraction, which means the precipitation dominates the chemical effects, keeps increasing steadily in the early, intermediate and late time.

The combined mechanical and chemical effects with respect to time may be further illustrated as figure 6. It shows the mechanical and chemical states as

function of time for one grid block close to the well. The mean effective stress decreased immediately at the beginning with negligible change at the later time, while the chemical precipitation keeps the nearly constant rate throughout the study time.

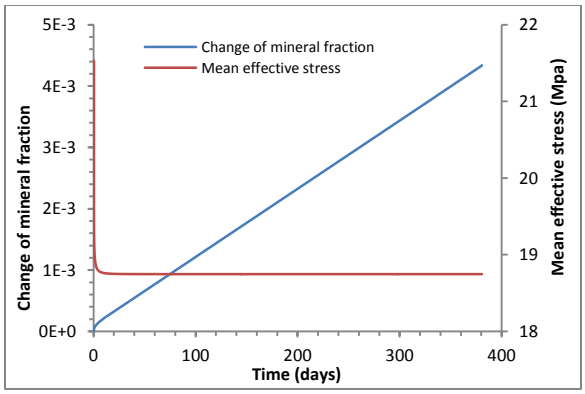


*Figure 6: The M and C effects on the grid block close to the wellbore*

The induced fracture aperture changes due to mechanical and chemical effect are calculated from the parameters in table 1 and plotted as figure 7. The decreasing effective stress leads to the enhancement on the facture but the mineral scaling counteracts this effect. At the early time the stress enhanced aperture outperforms the chemical precipitation, accordingly the total change of aperture $\Delta b$ is positive until 40 days. As analyzed before, mechanical process only dominates at the early time, the enhanced aperture decrease from the starting time due to stable precipitation process. Consequently the change of aperture becomes negative, less than the initial size of aperture, in the intermediate and late time. On the other hand, the chemical effect acts on closer area and mechanical effect on the further area, which explains the aperture sharp decrease around the well and fracture enhancement still exists at the radius of more than 30m after one year THMC process.

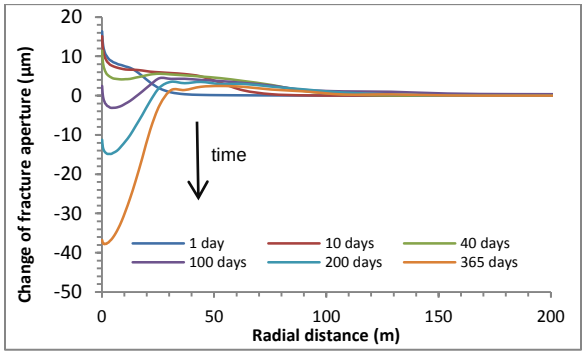


*Figure 7: Fracture aperture evolution due to M and C effects*

In order to identify the specific minerals responsible for the precipitation, the change of volume fraction for each mineral on the grid block close to the well is plotted as figure 8. The amorphous silica and albite-low are the top two minerals for precipitation process while calcite and clinochlore account for the main dissolution process.

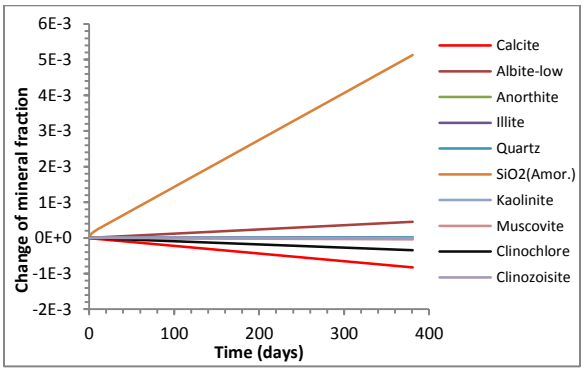


*Figure 8: Change of each mineral fraction of the grid block close to the wellbore*

**Case 1: Changed Chemical Composition**

Since $SiO_2$ leads the chemical precipitation, we reduce the aqueous silica concentration from 705 ppm ($1.1734\times10^{-2}$ mol/l) to 650 ppm ($1.0818\times10^{-2}$ mol/l) with same other conditions to formulate the case 2.

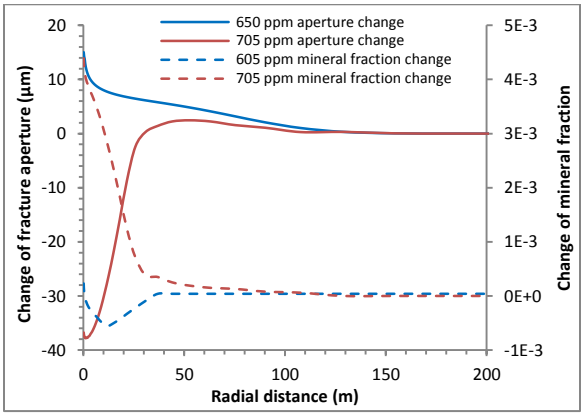


*Figure 9: Fracture aperture change and mineral fraction change after 365 days*

Figure 9 shows the changes of total aperture and mineral fraction after 365 day simulation for base case and lower $SiO_2$ case. The decrease by 55 ppm of $SiO_2$ in the injection water leads to the significant difference. The change of mineral fraction becomes negative in most areas except that immediately close to the well, which means the dissolution of mineral dominates the chemical process. Accordingly, the fracture aperture is enhanced by both mechanical and chemical effects.

**Case 2: Reduced temperature**

The temperature of the injection water has impacts on both mechanical and chemical process. The case 2 has the reduced temperature of 120 ºC of the injection water but with the same chemical composition as the base case.

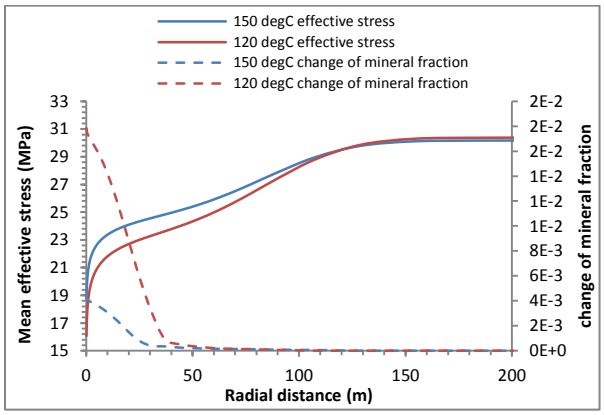


*Figure 10: Mean effective stress and the change of mineral fraction after 365 days*

Figure 10 shows the mechanical and chemical state after 365 days by comparing the base case and the reduced temperature case. The mean effective stress decreases by 1.5 MPa in the areas within 100m of radial distance, which could strengthen the enhanced effects on the fracture aperture. However, the lower injection temperature also results in larger increase in the mineral fraction, which means the precipitation reactions are stronger. Thus the temperature decrease leads to the different directions on aperture change for mechanical and chemical effects.

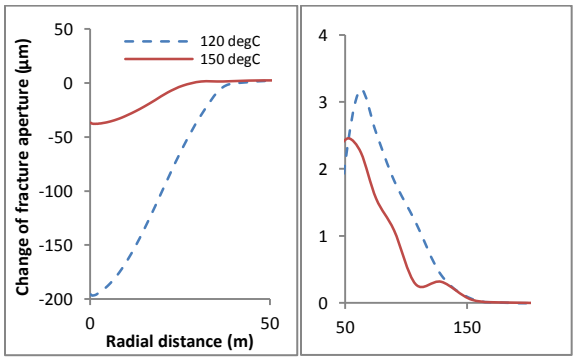


*Figure 11: Change of fracture aperture due to mechanical and chemical effects under reduced injection temperature after 365 days*

Figure 11 compares the change of fracture aperture between base case and the reduced temperature case. The left plot shows that the chemical precipitation results in the significant aperture decrease under lower injection temperature around the wellbore, less than 50m, even if the rock deformation could counteract this effect. However, the mechanical enhanced aperture could be observed beyond the radius of 50m in the right plot because the precipitation is weaker in those areas. The lower temperature leads to the stronger precipitation, meanwhile stronger mechanical enhanced aperture. The precipitation outperforms the mechanical induction in our example, but it may change for different values of material parameters, such as maximum mechanical fracture $b_m$, geometry aperture available for precipitation $b_g$, and mechanical constant $d$ in equation (31).

## CONCLUSIONS

A coupled THMC simulator has been developed for simulating the multiphase flow, heat transfer, rock deformation and chemical reactions in EGS reservoirs. In the model, fluid and heat flow is fully coupled with geomechanical model since the mean normal stress, solved simultaneously with fluid and heat flow equations. The chemical reaction model is sequentially coupled after the flow equations, solved at each time step. The solute transport and chemical reactions are solved iteratively until the chemical variable converges.

The mechanical model is based on the mean stress formulation and therefore cannot handle the shear-stress induced phenomena, such as rock failure by shearing. But it is sufficient and rigorous to simulate the stress induced reservoir evolution, such as porosity and permeability change, formation subsidence etc.

The application example illustrates the reservoir evolution in the vicinity areas of the injection well due to THMC effects. It is found that the mechanical effects act on the reservoir immediately from the start and the stress state becomes stable quickly, while the chemical effects accumulate steadily from beginning to the intermediate and late time. It is also observed that the mechanical effects reach further distance from the injection wells, while the mineral dissolution and precipitation concentrates around the injector.

The chemical composition and temperature of injected water are two key factors influencing the mechanical and chemical process. By optimizing the concentration of chemical components of injected water, the precipitation effects could be minimized or even eliminated while maintaining the mechanical enhanced fracture network. The temperature change has the opposite impacts on the mechanical and chemical process. For example, the reduced temperature helps the mechanical enhanced fracture but leads stronger mineral precipitation. Whether the

temperature change favors or undermines the fracture network under both mechanical and chemical effects may also depend on the material properties of the specific reservoir.

## ACKNOWLEDGEMENT

This work is supported by the U.S. Department of Energy under Contract No. DE-EE0002762, "Development of Advanced Thermal-Hydrological-Mechanical-Chemical (THMC) Modeling Capabilities for Enhanced Geothermal Systems". Special thanks are due to the Energy Modeling Group (EMG) of Department of Petroleum Engineering at Colorado School of Mines.

## REFERENCES

Bai, Mao, and Jean-Claude Roegiers. (1994), "Fluid flow and heat flow in deformable fractured porous media." *International journal of engineering science* **32**, no. 10: 1615-1633.

Davies, J. P., and D. K. Davies. (2001), "Stress-dependent permeability: characterization and modeling." *SPE Journal*, **6**.2 : 224-235.

Fakcharoenphol, Perapon, and Yu-Shu Wu. (2011), "A Coupled Flow-Geomechanics Model for Fluid and Heat Flow for Enhanced Geothermal Reservoirs." *In 45th US Rock Mechanics/Geomechanics Symposium.*

Jaeger, J. C., N. G. W. Cook, and R. W. Zimmerman. (2007), "Fundamentals of rock mechanics." *Blackwell, Fourth edition*.

Kiryukhin, A., Xu, T., Pruess, K., Apps, J., & Slovtsov, I. (2004), "Thermal–hydrodynamic–chemical (THC) modeling based on geothermal field data." *Geothermics*, **33**(3), 349-381.

Lasaga, A. C. (1984), "Chemical kinetics of water-rock interactions", *J. Geophys. Res.*, v.**89**, p. 4009-4025.

Lasaga, A. C., et al. (1994), "Chemical weathering rate laws and global geochemical cycles." *Geochimica et Cosmochimica Acta*, **58.**10: 2361-2386.

McKee, C. R., A. C. Bumb, and R. A. Koenig. (1988), "Stress-dependent permeability and porosity of coal and other geologic formations." *SPE formation evaluation*, **3**.1: 81-91.

Montalvo, F., Xu, T., & Pruess, K. (2005), "TOUGHREACT Code Applications to Problems of Reactive Chemistry in Geothermal Production-injection Wells. First Exploratory Model for Ahuachapán and Berlín Geothermal Fields." *In Proceedings of World Geothermal Congress 2005 Antalya, Turkey*.

Narasimhan, T. N., and P. A. Witherspoon. (1976), "An integrated finite difference method for analyzing fluid flow in porous media." *Water Resources Research*, **12**.1: 57-64.

Ostensen, R. W. (1986), "The effect of stress-dependent permeability on gas production and well testing." *SPE Formation Evaluation*, **1**.3: 227-235.

Pruess, K., Oldenburg, C., and G. Moridis, (1999), "TOUGH2 user's guide, Version 2.0," *Lawrence Berkeley Laboratory Report LBL-43134*, Berkeley, CA.

Pruess, K. and T.N. Narasimhan. (1985), "A Practical Method for Modeling Fluid And Heat Flow in Fractured Porous Media," *Soc. Pet. Eng. J.*, **25**, 14-26.

Rutqvist, J., Y-S. Wu, C-F. Tsang, and G. Bodvarsson. (2002), "A Modeling Approach for Analysis of Coupled Multiphase Fluid Flow, Heat Transfer, and Deformation in Fractured Porous Rock." *International Journal of Rock Mechanics and Mining Sciences* **39**, no. 4: 429-442.

Snow, David T. (1969), "Anisotropies permeability of fractured media." *Water Resources Research* **5**.6: 1273-1289.

Steefel, C. I., and Lasaga, A. C. (1994), "A coupled model for transport of multiple chemical species and kinetic precipitation/dissolution reactions with applications to reactive flow in single phase hydrothermal system." *Am. J. Sci*., v**. 294**, p. 529-592.

Takeno, Naoto, Tsuneo Ishido, and JW. Pritcheit. (2000), "Dissolution, transportation, and precipitation of silica in geothermal systems." *Rep Geol Surv Jpn* **284** :235-248.

Taron, Joshua, Derek Elsworth, and Ki-Bok Min. (2009), "Numerical simulation of thermal-hydrologic-mechanical-chemical processes in deformable, fractured porous media." *International Journal of Rock Mechanics and Mining Sciences*, **46**, no. 5: 842-854.

Tsang, Chin-Fu. (1999), "Linking Thermal, Hydrological, and Mechanical Processes in Fractured Rocks 1." *Annual review of earth and planetary sciences* **27,** no. 1 359-384.

Wang, Xiaonan, and Ahmad Ghassemi. (2012), "A 3D THERMAL-POROELASTIC MODEL FOR GEOTHERMAL RESERVOIR STIMULATION." *PROCEEDINGS, Thirty-Seventh Workshop on Geothermal Reservoir*

*Engineering Stanford University*, Stanford, California.

Winterfeld, P.H., Wu, Y.S. (2011), "Parallel simulation of CO2 sequestration with rock deformation in saline aquifers." *Society of Petroleum Engineers, SPE 141514.*

Witherspoon, P. A., J. S. Y. Wang, K. Iwai, and J. E. Gale. (1979), "Validity of cubic law for fluid flow in a deformable rock fra*cture." Technical Rep. No. LBL-9557, SAC 23.*

Xu, T., Ontoy, Y., Molling, P., Spycher, N., Parini, M., & Pruess, K. (2004a), "Reactive transport modeling of injection well scaling and acidizing at Tiwi field, Philippines." *Geothermics*, **33**(4), 477-491.

Xu, Tianfu, Eric Sonnenthal, Nicolas Spycher, and Karsten Pruess. (2004b), "TOUGHREACT User's Guide: A Simulation Program for Non-isothermal Multiphase Reactive Geochemical Transport in Variably Saturated Geologic Media." *V1. 2.1. No. LBNL-55460-2004. Ernest Orlando Lawrence Berkeley National Laboratory*, Berkeley, CA (US).

Zhang, Ronglei, Xiaolong Yin, Yu-Shu Wu, and Philip Winterfeld. (2012) "A Fully Coupled Model of Nonisothermal Multiphase Flow, Solute Transport and Reactive Chemistry in Porous Media." *In SPE* 2012 *Annual Technical Conference and Exhibition*.